Journal of Alloys and Compounds, 653 (2015) 546-551
http://dx.doi.org/10.1016/j.jallcom.2015.09.074

Influence of hot compaction on microstructure and magnetic properties of mechanically alloyed Fe(Co)-based amorphous compositions

J.J. Ipus[1], J.M. Borrego[1], J.S. Blázquez[1], M. Stoica[2,3], V. Franco[1], A. Conde[1]

[1] Departamento de Física de la Materia Condensada, ICMSE-CSIC, Universidad de Sevilla, P.O. Box 1065, 41080, Sevilla, Spain

[2] IFW Dresden, Institute for Complex Materials, D-01069, Dresde, Germany

[3] Politehnica University Timisoara, 300006, Timisoara, Romania

Abstract

Amorphous $Fe_{75}Nb_{10}B_{15}$ and $(Fe_{70}Co_{30})_{75}Nb_{10}B_{15}$ alloys were prepared by mechanical alloying from the elemental constituents and hot compacted at different temperatures within the supercooled liquid region. After compaction, the microstructure studied by X-ray diffraction shows an increase in the crystalline fraction for both compositions. Magnetic properties and magnetic entropy change of compacted samples of the Co-free alloy were enhanced with respect to the powder sample, meanwhile, a deterioration in these properties was observed for the Co containing alloy after compaction. Both changes could be ascribed to an enrichment in boron in the amorphous phase.

Keywords: Amorphous and nanocrystalline alloys, Mechanical alloying, Hot compaction, Magnetocaloric effect

Corresponding author: Javier S. Blázquez

e-mail: jsebas@us.es

Journal of Alloys and Compounds, 653 (2015) 546-551
http://dx.doi.org/10.1016/j.jallcom.2015.09.074

Introduction

Nanocrystalline and/or amorphous alloys have received large attention from the scientific community in the last years due to their attractive physical properties (mechanical, magnetic, etc), Particularly, Hitperm type alloys [1] were developed in 1998 to extend the good soft magnetic properties presented by Nanoperm type alloys [2] developed in the 80's to higher temperatures, as the Co addition increases the magnetic moment and the Curie temperature of both the amorphous and the crystalline phases [3].

These systems have been commonly prepared by rapid quenching techniques. However, mechanical alloying has become an important tool in materials science as an alternative route to directly prepare these amorphous and nanocrystalline microstructures in a wider compositional range [4]. Through this technique, starting from a mixture of pure elements or prealloyed materials, it is possible to process easily and economically a large amount of powder, which is an advantage from the commercial applications point of view. For example, although Co-based bulk amorphous samples have been produced by rapid solidification techniques such as copper mold casting [5,6,7], bulk samples with shapes and dimensions that cannot be obtained by direct casting have been successfully produced by powder compaction [8,9].

In fact, to obtain bulk amorphous and/or nanocrystalline samples in order to cover practical needs, powder should be compacted after milling. Compaction of amorphous powders into a bulk sample preserving the initial microstructure is a primary requirement but difficult to perform. Pressing at room temperature usually leads to mechanical degradation of the compacts and high temperature compaction is needed to obtain good interparticle binding. The use of a binding material enhances the mechanical stability of the compact but generally deteriorates its magnetic properties, as the amount of magnetic material is reduced. It is worth noting that applying high temperatures during compaction could lead to an undesirable coarsening of the crystals and even crystallization of the amorphous phase.

In this work, two amorphous Fe(Co)NbB alloys are prepared by mechanical alloying. Bulk samples were obtained by hot pressing within the supercooled liquid region without the use of any binding material. Microstructure and magnetic properties as a function of the compaction temperature are studied and compared to those of the as-milled powders.

Journal of Alloys and Compounds, 653 (2015) 546-551
http://dx.doi.org/10.1016/j.jallcom.2015.09.074

Experimental

Amorphous $(Fe_{1-X}Co_X)_{75}Nb_{10}B_{15}$ (X=0, 0.30) alloys were prepared via mechanical alloying starting from pure crystalline Fe, Nb and Co and intermetallic FeB powders in order to enhance the incorporation of hard boron into the matrix [10]. Milling was performed in a planetary mill Fritsch Pulverisette 4 Vario, with steel balls (10 mm diameter) and hardened steel vials (250 cm^3), initial powder mass of 30 g and a ball to powder ratio of 10:1. The rotational speed of the disc which supports the vials was 350 rpm and that of the vials was 700 rpm in opposite direction. Powder samples were taken out to study their microstructure, thermal stability and magnetic properties after 20 and 40 h milling. Disk-shaped samples 10 mm diameter and 4 mm thick were prepared by compaction of powders using an uniaxial hot press under a vacuum of 10^{-3} Pa. The powder was heated at 0.67 K s^{-1} up to the consolidation temperature, compacted under a pressure of 700 MPa for 1.5 min and then cooled down to room temperature using Ar flow. Density of the compacted samples, obtained from Archimedes method, shows, for $(Fe_{0.7}Co_{0.3})_{75}Nb_{10}B_{15}$ alloy, an increase from 5.3±0.4 g/cm^3 for the sample compacted at 753 K to 6.9±0.5 g/cm^3 for sample compacted at higher temperatures. In the case of the Co-free alloy, density increases from 6.1±0.4 g/cm^3 for the sample compacted at 773 K to 6.9±0.5 g/cm^3 for sample compacted at higher temperatures. This indicates about 90 % of the expected density for a bulk amorphous sample of these compositions.

Microstructural characterization was studied by X-ray diffraction using Cu-Kα radiation in a Bruker D8I diffractometer and scanning electron microscopy using a Zeiss Auriga Crossbeam Focused Ion Beam (FIB)-Scanning Electron Microscopy (SEM). SEM images were taken on in situ polished surfaces using Ga ion beam in FIB mode. Thermal characterization of the samples was studied by differential scanning calorimetry (DSC) using a Perkin Elmer DSC7 at a heating rate of 20 K/min in a continuous Ar flow. Magnetic properties were studied using a Lakeshore 7407 vibrating sample magnetometer with a maximum applied magnetic field of 1.5 T. Isothermal magnetization curves were measured on parallelepipeds of about 1x1x3 mm in size in a temperature range from 100 to 753 K with increments of 10 K. Spontaneous specific magnetization, σ_0, was obtained from the extrapolation of high field magnetization curves to zero field. Curie temperature,

Journal of Alloys and Compounds, 653 (2015) 546-551
http://dx.doi.org/10.1016/j.jallcom.2015.09.074

T_C, was calculated as the inflexion point of σ_0(T) curves. Hysteresis loops as a function of temperature were recorded in a temperature range of 100-753 K with steps of 50 K.

Isothermal magnetic entropy change, ΔS_M, due to the application of a magnetic field, was calculated by processing the temperature and field dependent magnetization curves using a numerical approach to the expression:

$$\Delta S_M = \mu_0 \int_{H_1}^{H_2} \left(\frac{\partial M}{\partial T} \right)_H dH \,, \tag{1}$$

where M is the magnetization and T the temperature and H_1 and H_2 are the minimum and maximum applied fields. The partial derivatives are replaced by finites differences and the integration is performed numerically. This procedure was performed with the help of the Magnetocaloric Effect Analysis Program [11]. The bulk samples were cut into small parallelepipeds and its longest axis was aligned with the applied field to minimize the demagnetizing field. In the case of powder samples the unavoidable demagnetizing factor, N_D, is considered as 1/3 [12] for loosely packed spherical samples, in order to correct the isothermal magnetization curves as:

$$H = H_{app} - N_D M \,, \tag{2}$$

where H_{app} is the applied magnetic field and H is the internal field. The refrigerant capacity represents a measure of the energy transferred between the hot and cold reservoirs. In this study the refrigerant capacity, RC_{FWHM}, was calculated as the product of the peak magnetic entropy change times the full width at half maximum of the peak.

Results and Discussion

The microstructural evolution of powder samples was followed by XRD. Figure 1 shows the XRD patterns of samples after 20 and 40 h milling for both studied compositions, along with the deconvolution (a Gausssian profile to describe the amorphous halo and a Lorentzian profile for the nanocrystalline α-Fe type phase) used to extract the fraction of phases from the patterns when possible. It is shown that, after the formation of the bcc Fe-Co(NbB) supersaturated solid solution, the development of an amorphous phase takes place and its fraction increases as the crystalline one decreases.

Journal of Alloys and Compounds, 653 (2015) 546-551
http://dx.doi.org/10.1016/j.jallcom.2015.09.074

An almost completely amorphous material is obtained for $Fe_{75}Nb_{10}B_{15}$ alloy after 20 h milling and for the $(Fe_{0.7}Co_{0.3})_{75}Nb_{10}B_{15}$ alloy after 40 h. DSC records presented in figure 2a show the thermal stability of the powder samples after 40 h for both compositions. Different processes can be observed in the scans. At low temperatures, a gas desorption process starting at ~390 K followed by a broad structural relaxation process at ~500 K. Both features are typically observed in powder samples [13]. Although it is not fully accepted the existence of glass transition for amorphous systems not obtained by rapid quenching, an exothermic feature is observed that could be named as T_g (inset of Fig. 2a) and estimated at T_g ~760 and 785 K for $(Fe_{0.7}Co_{0.3})_{75}Nb_{10}B_{15}$ and $Fe_{75}Nb_{10}B_{15}$ alloys, respectively, and the onset temperature of the main crystallization process was measured at T_{on} ~815 and 850 K for $(Fe_{0.7}Co_{0.3})_{75}Nb_{10}B_{15}$ and $Fe_{75}Nb_{10}B_{15}$samples, respectively.

In order to perform the hot compaction of the powder samples, one of the targets was to retain the previously observed microstructure of the initial powder. Therefore, temperatures close but below the crystallization temperatures were selected for compaction: 753, 773 and 793 K for $(Fe_{0.7}Co_{0.3})_{75}Nb_{10}B_{15}$ alloy and 773, 793, 803 and 813 K for $Fe_{75}Nb_{10}B_{15}$ alloy. A compromise has been taken between the heating rate of the hot-press (limited to 0.67 K/min) and the DSC heating rate needed to get a significant signal to noise ratio. A range of temperatures has been explored to minimize the influence of the different rates on the conclusions derived.

After compaction, the microstructure of bulk samples was examined by XRD and the same deconvolution procedure used for the case of as-milled powder was applied to the compacted samples, as shown in figure 1. Lattice parameter does not present significant changes with compaction (a=2.878±0.005 Å for both compositions). All values are higher than that of pure bcc-Fe. This fact could be explained by the influence of Nb atoms into the lattice. [14,15].

After hot compaction, whereas for the $Fe_{75}Nb_{10}B_{15}$ sample X_C increases up to ~0.10 regardless compaction temperature, for the $(Fe_{0.7}Co_{0.3})_{75}Nb_{10}B_{15}$ sample X_C continuously increases with temperature, reaching ~0.16 for the sample compacted at 793 K. This increment in X_C is in agreement with the closer proximity of the compaction temperature to the crystallization temperature in $(Fe_{0.7}Co_{0.3})_{75}Nb_{10}B_{15}$ (ΔT =22 K) than in $Fe_{75}Nb_{10}B_{15}$ alloy (ΔT =37 K).

Journal of Alloys and Compounds, 653 (2015) 546-551
http://dx.doi.org/10.1016/j.jallcom.2015.09.074

DSC scans showing the thermal stability of compacted samples are presented in figures 2b-c. From these scans we can see that the low temperature processes, T <750 K, observed in powder samples and ascribed to microstuctural relaxation, have disappeared for all compacted samples. Moreover, no important changes in the peak temperature are observed after compaction for $Fe_{75}Nb_{10}B_{15}$ alloy. For the $(Fe_{0.7}Co_{0.3})_{75}Nb_{10}B_{15}$ alloy, whereas for samples compacted at 753 and 773 K no significant changes are observed in the peak temperatures, an increase of ~10 K is detected for the sample compacted at 793 K. This change in the crystallization temperature for the $(Fe_{0.7}Co_{0.3})_{75}Nb_{10}B_{15}$ alloy could be ascribed to a partial consumption of the transformation due to crystallization of the bcc-(FeCo) type phase. Moreover, small compositional changes in the amorphous phase (e.g. an enrichment in boron content) during compaction at the highest temperature could also lead to an increase in the crystallization temperature of the FeCo-based amorphous alloys [16].

Coercivity, H_C, at room temperature shows a reduction after compaction from ~2 and ~4 kA/m for $Fe_{75}Nb_{10}B_{15}$ and $(Fe_{0.7}Co_{0.3})_{75}Nb_{10}B_{15}$ powders, respectively, down to ~1 kA/m for both compositions. This drop in H_C could be ascribed to relaxation phenomena in the samples due to annealing during compaction. Spontaneous specific magnetization values of compacted samples present different behaviors for each alloy. For the $Fe_{75}Nb_{10}B_{15}$ alloy at room temperature a continuous increase from ~46 emu/g (powder) up to ~54 emu/g (compacted at 813 K) with compaction temperature is observed. However, for the $(Fe_{0.7}Co_{0.3})_{75}Nb_{10}B_{15}$ alloy no important changes in σ_0 are observed at room temperature.

The temperature dependence of σ_0 is presented in figure 3 for the different samples. It is observed that T_C for the $(Fe_{0.7}Co_{0.3})_{75}Nb_{10}B_{15}$ alloy does not change after compaction at 753 and 773 K with respect to the value observed for the powder sample, with T_C =563 K. However, a reduction down to T_C =533 K for the sample compacted at 793 K is observed. For the $Fe_{75}Nb_{10}B_{15}$ samples, T_C increases from 320 K, for the powder sample, up to 340 K for each compacted sample from 773 K to 803 K, but a smaller increase (T_C =330 K) is observed for the sample compacted at 813 K. These features could be related to compositional changes (a better dissolution of boron) in the amorphous matrix during the compaction. In fact, an increase in boron content in amorphous Fe-B leads to an increase in T_C of ~20 K/at.% B [17], as well as an increase in σ_0 [18]. In the case of Co-B amorphous alloys, a decrease of ~30 K/at.% B in T_C is reported [19].

Journal of Alloys and Compounds, 653 (2015) 546-551
http://dx.doi.org/10.1016/j.jallcom.2015.09.074

Figure 4 shows the temperature dependence of coercivity for $Fe_{75}Nb_{10}B_{15}$ sample compacted at 813 K. All samples exhibit a similar behavior. An initial increase of the coercivity can be seen as the measurement temperature reaches T_C and then a decrease is observed for higher temperatures. The initial trend can be explained by a suppression of the exchange coupling in between the remaining nanocrystals as the amorphous matrix become paramagnetic. Above the Curie temperature of the amorphous phase, the gradual disappearance of the dipolar coupling between nanocrystals causes a reduction in coercivity as they approach the superparamagnetic regime as temperature increases [20].

The temperature dependence of the magnetic entropy change, ΔS_M, for a magnetic field change of 1 T is shown in figure 5 for all studied samples. It can be seen that, after compaction, a ~15 K increase of the peak temperature takes place for the $Fe_{75}Nb_{10}B_{15}$ alloy. For the $(Fe_{0.7}Co_{0.3})_{75}Nb_{10}B_{15}$ alloy the peak temperature shows a reduction of ~20 K only for the sample compacted at the highest temperature. The peak temperature, T_{pk}, as a function of the compacted one, T_{comp}, for both alloys is presented in figure 6a. The shift of the peak temperature for both alloys agrees with the shift observed in T_C and could be ascribed to the increase in B content in the amorphous phase during hot temperature compaction. In fact, an incorporation as small as ~0.7 at.% B in the amorphous matrix could explain the observed shifts of the peak temperature for both compositions as reported in [17,18].

The evolution of the peak value of ΔS_M and refrigerant capacity as a function of compaction temperature are presented in figure 6 (b and c). A continuous reduction in the peak value of $|\Delta S_M|$ for compacted $(Fe_{0.7}Co_{0.3})_{75}Nb_{10}B_{15}$ samples with respect to the as-milled one can be observed. However, for the case of $Fe_{75}Nb_{10}B_{15}$ alloy an increase of ~13% in the peak value of ΔS_M for compacted samples is observed. The continuous reduction for the $(Fe_{0.7}Co_{0.3})_{75}Nb_{10}B_{15}$ alloy after compaction could be ascribed to the progressive crystallization during hot compaction. In the other case, the increase observed for the $Fe_{75}Nb_{10}B_{15}$ samples after compaction can be explained by the effect of boron incorporation in the amorphous matrix which enhances the magnetic moment in Fe-based amorphous alloys [10,21], in agreement with the increase of T_C.

The refrigerant capacity shows two different behaviors for the two different compositions. In the case of $Fe_{75}Nb_{10}B_{15}$ alloy this value decreases with respect to that of powder sample, which is related to the sharpening of the ΔS_M curve due to a reduction of

Journal of Alloys and Compounds, 653 (2015) 546-551
http://dx.doi.org/10.1016/j.jallcom.2015.09.074

the T_C distribution with increasing compaction temperature, as normally observed for powder samples [22, 23, 24]. For the $(Fe_{0.7}Co_{0.3})_{75}Nb_{10}B_{15}$ alloy significant changes in RC are not initially observed but a large reduction is measured after compaction at 793 K, which can be explained by the reduction in the peak value of ΔS_M due to the partial crystallization of this sample.

There are two processes which cause B enrichment of the amorphous phase: crystallization of the α-Fe type phase and dissolution of the remnant boron inclusions. In the former case, after a 10 % crystallization the composition of the residual amorphous phase, neglecting the presence of B inclusions, should be $(FeCo)_{72}Nb_{11}B_{17}$, which could reasonably account for the boron enrichment. However, previous studies on Fe-Zr-B [25] report on the dissolution of boron inclusions after high temperature treatment. In order to consider this mechanism, SEM micrographs were obtained on cross sections of compacted samples after being polished using a beam of Ga ions. Figure 7 shows these SEM images at the lowest and highest compaction temperatures for $Fe_{75}Nb_{10}B_{15}$ (Fig. 7a and 7b) and $(Fe_{0.7}Co_{0.3})_{75}Nb_{10}B_{15}$ alloy (7c-7d), respectively. B inclusions are still clearly observed as dark spots (regions of low interaction with electrons due to the low atomic number of B atoms) in the compacted samples, even at the highest compaction temperature, and not significant changes are evident with respect to the samples compacted at lower temperatures. However, slight boron incorporation from the inclusions, below our resolution, cannot be discarded.

Conclusions

Mechanically alloyed $Fe_{75}Nb_{10}B_{15}$ and $(Fe_{0.70}Co_{0.30})_{75}Nb_{10}B_{15}$ powder compositions were hot compacted at different temperatures and the evolution of the microstructural and magnetic properties were studied.

Around 10 % crystalline fraction was developed after compaction within the supercooled liquid region for $Fe_{75}Nb_{10}B_{15}$ samples. For the $(Fe_{0.70}Co_{0.30})_{75}Nb_{10}B_{15}$ samples a continuous increase up to X_C ~16% was observed.

The magnetic properties show changes with the compaction temperature for both compositions. Small increases in the room temperature spontaneous specific magnetization, the Curie temperature and the peak value of the magnetic entropy change

Journal of Alloys and Compounds, 653 (2015) 546-551
http://dx.doi.org/10.1016/j.jallcom.2015.09.074

for the $Fe_{75}Nb_{10}B_{15}$ alloy were observed. For the case of $(Fe_{0.7}Co_{0.3})_{75}Nb_{10}B_{15}$ alloy a reduction in T_C and the peak value of the magnetic entropy change was evidenced, while σ_0 is almost constant. In both cases, changes in T_C could be explained after a small boron enrichment of the amorphous phase during compaction. Crystallization of the α-Fe type phase can explain the enhancement of σ_0 in $Fe_{75}Nb_{10}B_{15}$ alloy as well as its constant value in $(Fe_{0.7}Co_{0.3})_{75}Nb_{10}B_{15}$ alloy while the peak value of $|\Delta S_M|$ decreases.

Acknowledgements

This work was supported by the Spanish Ministry of Science and Innovation (MICINN) and EU FEDER (project MAT2013-45165-P) and the PAI of the Regional Government of Andalucía.

References

[1] M.A. Willard, D.E. Laughlin, M.E. McHenry, D. Thoma, K. Sickafus, J.O. Cross, V.G. Harris, J. Appl. Phys. 84 (1998) 6773-6677.

[2] K. Suzuki, N. Kataoka, A. Inoue, A. Makino, T. Matsumoto, Mater. Trans. JIM 31 (1990) 743-746.

[3] M.E. McHenry, M.A. Willard, D.E Laughlin, Prog. Mater. Sci. 44 (1999) 291-433.

[4] C. Suryanarayana, Prog. Mater. Sci. 46 (2001) 1-184.

[5] A.H. Taghvaei, M. Stoica, K.G. Prashanth, J. Eckert, Acta Mater. 61 (2013) 6609-6621.

[6] K. Biswas, S. Ram, S. Roth, L. Schultz, J. Eckert, J. Mater. Sci. 41 (2006) 3445-3450.

[7] A. Inoue, Acta Mater. 48 (2000) 279-306.

[8] P. Kollar, J. Bednarcik, S. Roth , H. Grahl, J. Eckert, J. Magn. Magn. Mater. 278 (2006) 373-378.

[9] J. Fuezer, J. Bednarcik, P. Kollar, S.Roth, J. Magn. Magn. Mater. 316 (2007) E834-E887.

[10] J.J. Ipus, J.S. Blázquez, C.F. Conde, J.M. Borrego, V. Franco, S. Lozano-Pérez, A. Conde, Intermetallics 49 (2014) 98-105.

[11] V. Franco, B.C. Dodrill, C. Radu, Magnetics Business & Technology. Winter 2014, 13 (2014) 8. The analysis software and accompanying Application Note is available at: http://www.lakeshore.com/products/Vibrating-Sample-Magnetometer/pages/MCE.aspx

[12] L.M. Moreno, J.S. Blázquez, J.J. Ipus, J.M. Borrego, V. Franco, A. Conde, J. Appl. Phys. 115 (2014) 17A302.

[13] J.S. Blázquez, J.J. Ipus, C.F. conde, A. Conde, J. Alloy. Compd. (2012) S9-S12.

[14] J.J. Ipus, J.S. Blázquez, V. Franco, A. Conde, J. Alloy. Compd. 496 (2010) 7-12.

[15] J.J. Ipus, J.S. Blázquez, V. Franco, A. Conde, M. Krasnowski, T. Kulik, S. Lozano-Pérez, J. Appl. Phys. 107 (2010) 073901.

[16] Wijn HPJ. Landolt-Börnstein: Magnetische Eigenschaften von Metallen, vol1. 19. Berlin: Springer; 1991. P. 126.

[17] Wijn HPJ. Landolt-Börnstein: Magnetische Eigenschaften von Metallen, vol1. 19. Berlin: Springer; 1991. p. 100.

[18] Wijn HPJ. Landolt-Börnstein: Magnetische Eigenschaften von Metallen, vol1. 19. Berlin: Springer; 1991. p. 88.

[19] Wijn HPJ. Landolt-Börnstein: Magnetische Eigenschaften von Metallen, vol1. 19. Berlin: Springer; 1991. p. 126.

[20] V. Franco, C.F. Conde, A. Conde, L.F. Kiss, Phys. Rev. B 72 (2005) 174424:1-10.

[21] Wijn HPJ. Landolt-Börnstein: Magnetische Eigenschaften von Metallen, vol1. 19. Berlin: Springer; 1991. P. 92.

[22] J.J. Ipus, J.S. Blázquez, V. Franco, M. Stoica, A. Conde, J. Appl. Phys. 115 (2014) 17B518.

[23] L.M. Moreno-Ramírez, J.J. Ipus, V. Franco, J.S. Blázquez, A. Conde, J. Alloy. Compd. 622 (2015) 606-609.

[24] P. Alvarez-Alonso, J.L. Sánchez-Llamazares, C.F. Sánchez-Valdés, G.J. Cuello, V. Franco, P. Gorria, J.A. Blanco, J. Appl. Phys. 115 (2014) 17A929.

[25] L. Schultz, E. Hellstern, G. Zorn, Zeitschrift für Physikalische Chemie 157 (1988) 203-208.

Journal of Alloys and Compounds, 653 (2015) 546-551
http://dx.doi.org/10.1016/j.jallcom.2015.09.074

Figure captions

Figure 1. XRD patterns for powder samples after 20 and 40 h milling and compacted samples at different compaction temperatures for both compositions.

Figure 2. DSC scans at 20 K/min of (a) 40 h milled powders for both studied alloys and compacted samples at different temperatures for (b) $(Fe_{0.7}Co_{0.3})_{75}Nb_{10}B_{15}$ alloy and (c) $Fe_{75}Nb_{10}B_{15}$ alloy. Inset shows the supercooled liquid region.

Figure 3. Temperature dependence of magnetization for compacted samples.

Figure 4. Coercivity as a function of temperature for $Fe_{75}Nb_{10}B_{15}$ sample compacted at 813 K.

Figure 5. Temperature dependence of magnetic entropy change for compacted samples of both studied compositions. Values corresponding to powder samples are included.

Figure 6. Values of peak temperature of ΔS_M, T_{pk}, (a), maximum of the magnetic entropy change, $|\Delta S_M|$, (b) and refrigerant capacity, RC_{FWHM}, (c) as a function of compaction temperature, T_{Comp}. Values corresponding to powder samples are included. Solid symbols correspond to $(Fe_{0.7}Co_{0.3})_{75}Nb_{10}B_{15}$ alloy and open symbols to $Fe_{75}Nb_{10}B_{15}$ alloy.

Figure 7. Secondary electron images on a cross section polished using FIB milling. $Fe_{75}Nb_{10}B_{15}$ samples compacted at 773 K (a) and 813 K (b); and $(Fe_{0.7}Co_{0.3})_{75}Nb_{10}B_{15}$ samples compacted at 753 K (c) and 793 K (d).

Journal of Alloys and Compounds, 653 (2015) 546-551
http://dx.doi.org/10.1016/j.jallcom.2015.09.074

Figure 1.

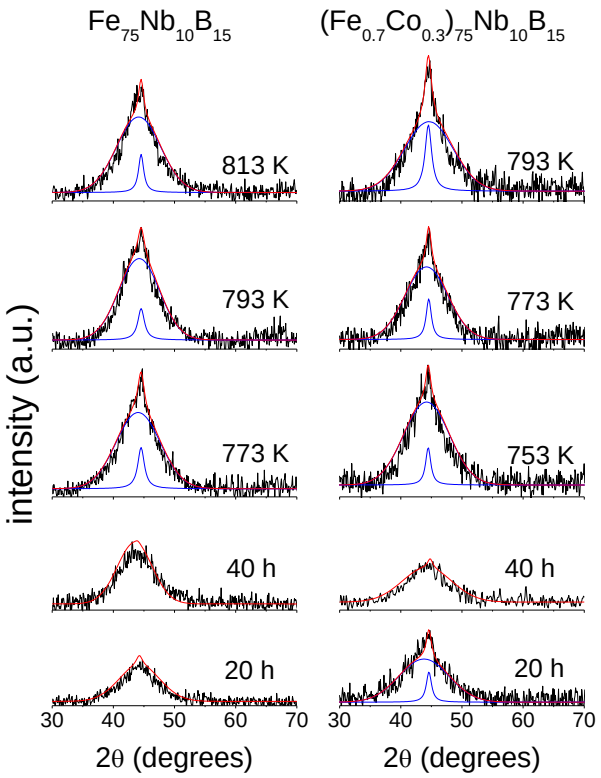

Journal of Alloys and Compounds, 653 (2015) 546-551
http://dx.doi.org/10.1016/j.jallcom.2015.09.074

Figure 2.

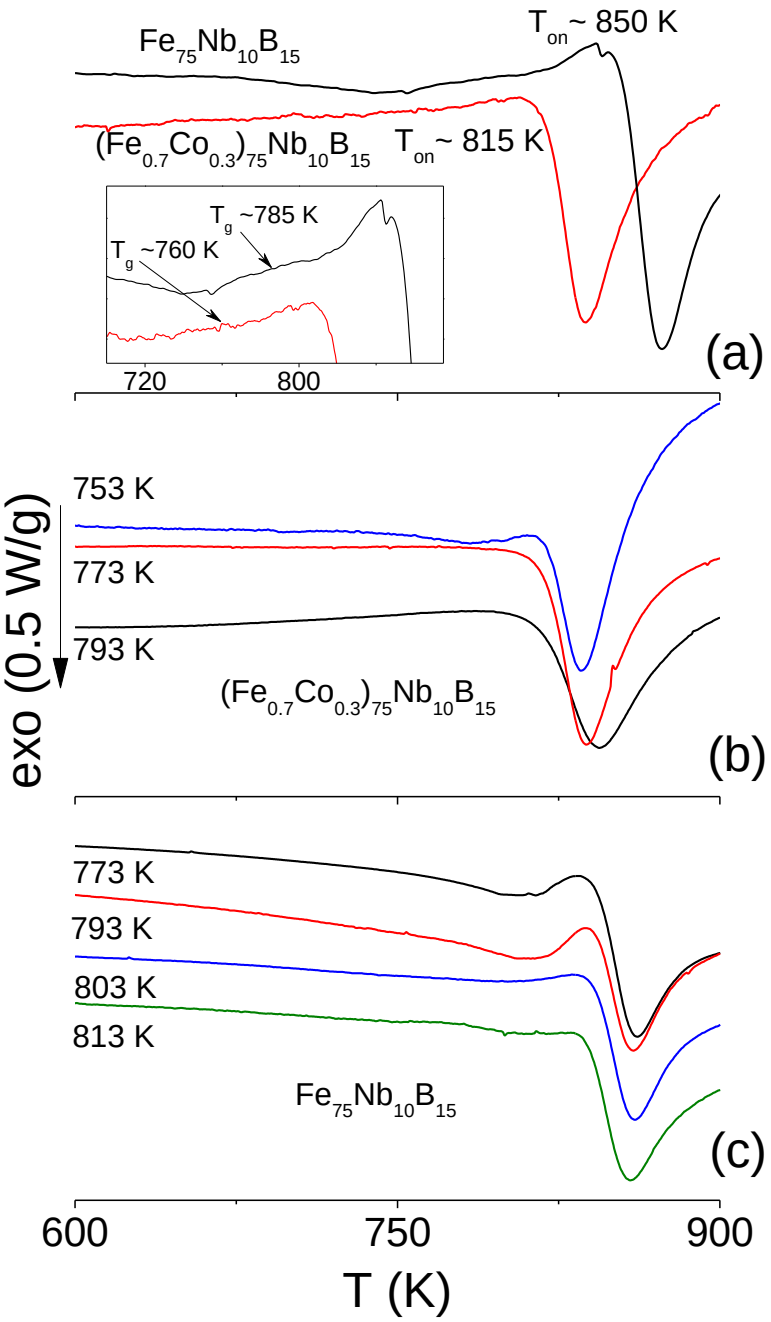

Journal of Alloys and Compounds, 653 (2015) 546-551
http://dx.doi.org/10.1016/j.jallcom.2015.09.074

Figure 3.

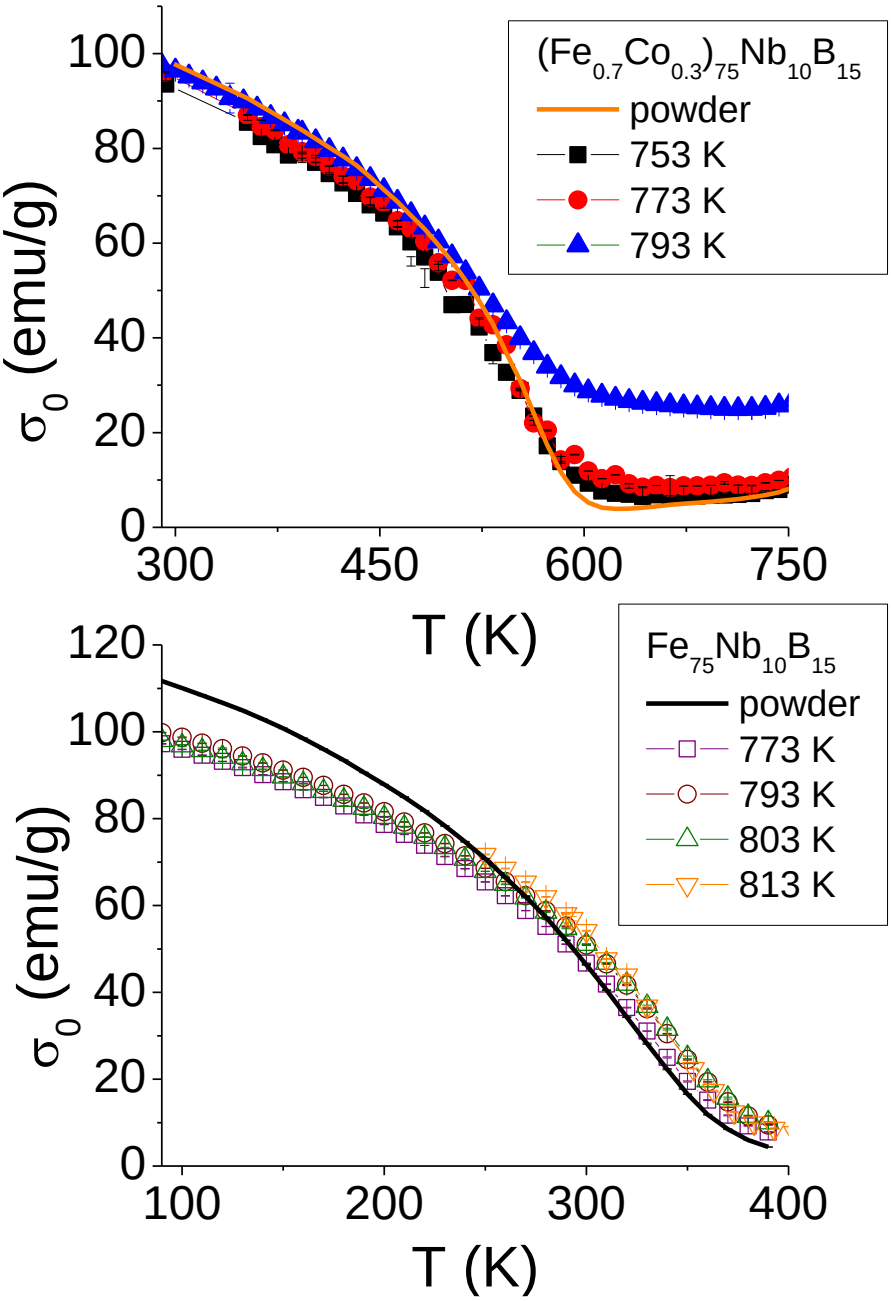

Journal of Alloys and Compounds, 653 (2015) 546-551
http://dx.doi.org/10.1016/j.jallcom.2015.09.074

Figure 4.

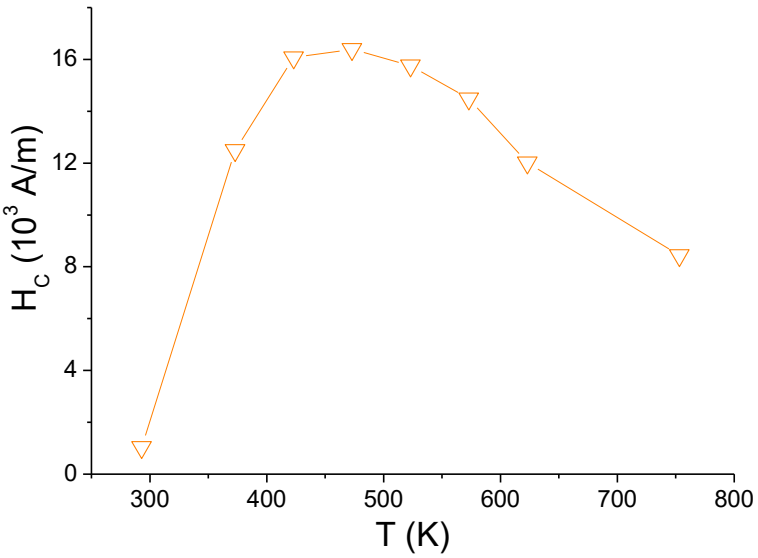

Journal of Alloys and Compounds, 653 (2015) 546-551
http://dx.doi.org/10.1016/j.jallcom.2015.09.074

Figure 5.

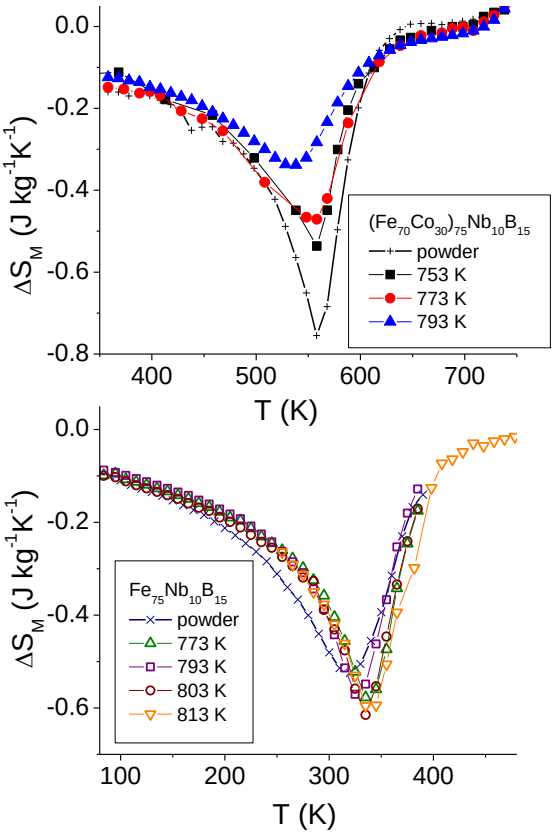

Journal of Alloys and Compounds, 653 (2015) 546-551
http://dx.doi.org/10.1016/j.jallcom.2015.09.074

Figure 6.

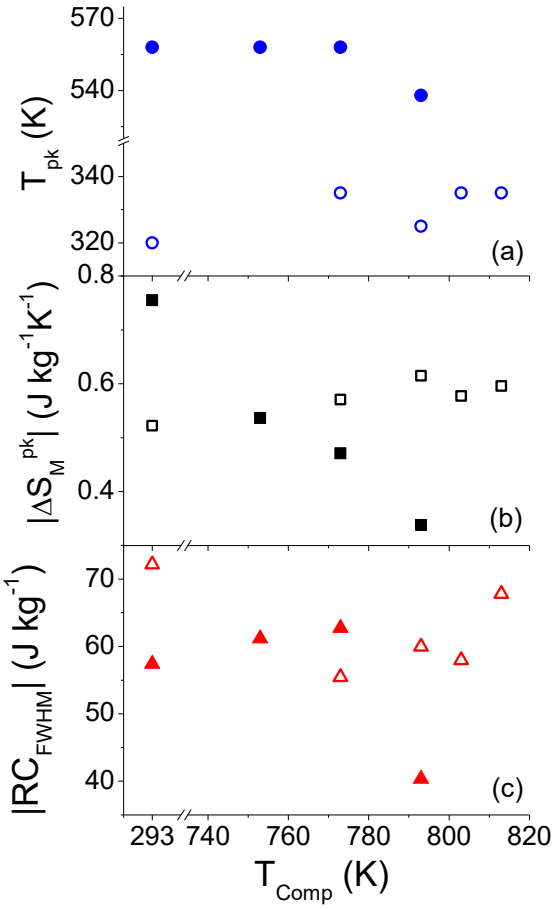

Journal of Alloys and Compounds, 653 (2015) 546-551
http://dx.doi.org/10.1016/j.jallcom.2015.09.074

Figure 7.